Mon. Not. R. Astron. Soc. **397,** 763–774 (2009) doi:10.1111/j.1365-2966.2008.14034.x

Axisymmetric magnetic fields in stars: relative strengths of poloidal and toroidal components

Jonathan Braithwaite★

Canadian Institute for Theoretical Astrophysics, 60 St. George Street, Toronto ON M5S 3H8, Canada

Accepted 2008 November 19. Received 2008 August 22; in original form 2008 June 18

ABSTRACT

In this third paper in a series on stable magnetic equilibria in stars, I look at the stability of axisymmetric field configurations and, in particular, the relative strengths of the toroidal and poloidal components. Both toroidal and poloidal fields are unstable on their own, and stability is achieved by adding the two together in some ratio. I use Tayler's stability conditions for toroidal fields and other analytic tools to predict the range of stable ratios and then check these predictions by running numerical simulations. If the energy in the poloidal component as a fraction of the total magnetic energy is written as E_p/E, it is found that the stability condition is $a(E/U) < E_p/E \lesssim 0.8$ where E/U is the ratio of magnetic to gravitational energy in the star and a is some dimensionless factor whose value is of order 10 in a main-sequence star and of order 10^3 in a neutron star. In other words, whilst the poloidal component cannot be significantly stronger than the toroidal, the toroidal field can be very much stronger than the poloidal–given that in realistic stars we expect $E/U < 10^{-6}$. The implications of this result are discussed in various contexts such as the emission of gravitational waves by neutron stars, free precession and a 'hidden' energy source for magnetars.

Key words: MHD – stars: chemically peculiar – stars: magnetic fields – stars: neutron – white dwarfs.

1 INTRODUCTION

Magnetic fields are observed in various types of star which are considered unlikely to harbour a suitable regenerative dynamo process because of the lack of convection. For instance, strong fields (300 G to 30 kG) are observed via the Zeeman effect on chemically peculiar main-sequence A stars (the Ap stars; see Mathys 2001, for a review), as well as on higher mass O and B stars. These stars do contain a small convective core and a magnetic field produced inside it could, in principle, rise through the radiative envelope in the form of buoyant flux tubes, but the time-scale of this process is almost certainly too long for anything to be seen on the surface within the star's lifetime (MacGregor & Cassinelli 2003). The magnetic white dwarfs (WDs, with observed fields of 10^4–10^9 G) have only weak surface convection, and neutron stars (NSs, with fields 10^8–10^{15} G) no convection at all. All of these stars must therefore contain a stable 'fossil' magnetic field, inherited either from the original molecular gas cloud or from the previous stage of evolution (e.g. WDs from the main sequence, see Wickramasinghe & Ferrario 2005, or NSs from a degenerate stellar core, see Ferrario & Wickramasinghe 2006) or left over from some kind of dynamo process at the time of formation, either during the pre-main-sequence phase, in the case of Ap stars, or during the convective protoneutron star phase (Duncan & Thompson 1992). To have survived since this time, a field must be stable on a dynamic (Alfvén) time-scale.[1] It was suggested by Prendergast (1956) that a stellar magnetic field in stable equilibrium must contain both poloidal (meridional) and toroidal (azimuthal) components, since both are unstable on their own. It was then shown more rigorously by Tayler (1973) that any purely toroidal field configuration is unstable at least some place in a star, and by Wright (1973) and Markey & Tayler (1973, 1974) that any purely poloidal field is unstable. More recently, the properties of these instabilities of toroidal and poloidal fields have been looked at analytically and numerically (Spruit 1998; Braithwaite & Spruit 2006; Braithwaite 2006, 2007; Bonanno & Urpin 2008).

Analytic methods have proven useful in demonstrating the instability of various equilibrium configurations, but have not been as useful in demonstrating the existence of any stable configuration. Numerical simulations (Braithwaite & Nordlund 2006, hereafter Paper I; see also Braithwaite & Spruit 2004) showed that an arbitrary initial magnetic field inside a non-convective star can evolve on an Alfvén time-scale into a stable configuration. A roughly axisymmetric configuration was found of a mixed poloidal–toroidal twisted-torus shape as shown in Fig. 1. Once formed it continues to evolve as a result of diffusive processes such as finite conductivity, on a much longer time-scale. For instance, the diffusion time-scale

[1] The solid crust of a NS can hold an otherwise unstable field in place, provided that the field strength is below some threshold $\sim 10^{13}$ G, but it is not clear whether the crust forms soon enough after the end of the protoneutron star convective phase to prevent relaxation into stable equilibrium.

★E-mail: jon@cita.utoronto.ca

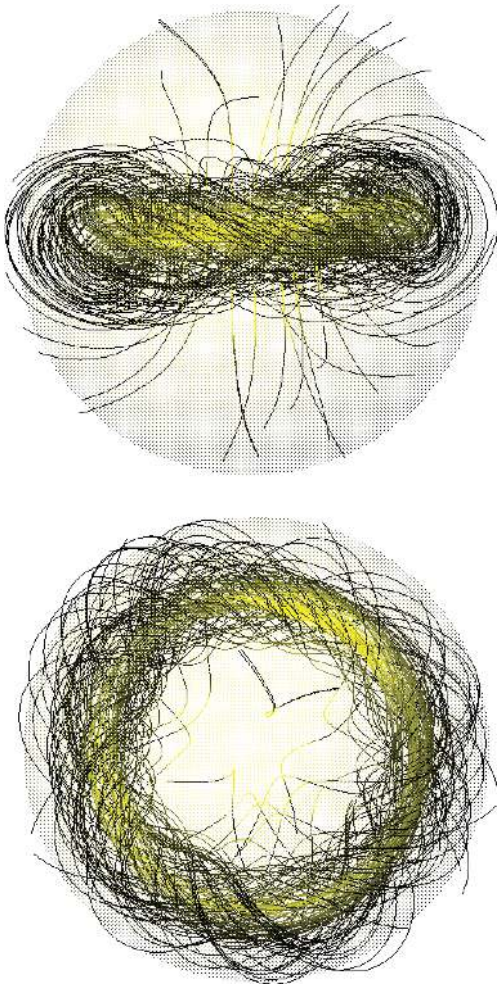

Figure 1. The shape of the stable twisted-torus field in a star, viewed from different angles. The transparent surface represents the surface of the star; strong magnetic field is shown with yellow field lines, weak with black.

is $\sim 10^{10}$ yr for an Ap star; in the case of a NS, this time-scale is much less certain and is a result of Hall drift and other processes as well as Ohmic dissipation. As the field evolves it moves outwards, passing quasi-statically through a series of stable equilibria until, upon reaching the end of the series of axisymmetric equilibria, it changes to a non-axisymmetric equilibrium. These non-axisymmetric equilibria are described in more detail in Braithwaite (2008, hereafter Paper II), where it was also found that a non-axisymmetric equilibrium can be formed on an Alfvén time-scale directly, from somewhat different initial conditions. Essentially, the important difference is the central concentration of the initial field and the fraction of flux connected through the stellar surface –a non-axisymmetric equilibrium can be formed directly from an initial field whose energy is more 'spread out' rather than concentrated towards the centre of the star, and which has significant flux connection through the stellar surface.

We are concerned here with only the axisymmetric class of equilibria. Since both toroidal and poloidal fields are unstable on their own, there is presumably some allowed range of ratios of the two respective field strengths; it is the principal purposes of this paper shed some light on what these stable ratios might be. The toroidal field is always confined to the interior of a star, since a toroidal field on or above the surface would require long-lived currents outside the star, so that we observe on the surface only the poloidal component. Therefore, it is either difficult or impossible to get any *direct* observational constraint on the range of allowed ratios. There are, however, some interesting ways in which a toroidal magnetic field can manifest itself indirectly, which make the question of allowed poloidal/toroidal ratios a useful line of study. First, in predominantly non-convective main-sequence stars (i.e. $>1.5\,M_{\odot}$) it would be useful to know how much flux may be hidden below the surface, since this flux may be important during formation, eventually be visible on the WD, be responsible for shaping the planetary nebula, affect the supernova explosion in some way, and affect the natal rotation periods of NSs and WDs via core-envelope coupling. In fact, this reminds us of another question: how much of the *poloidal* flux can be hidden below the surface? Certainly not all of it has to go through the stellar surface, but may be confined to the interior. This paper also sheds some light on this issue. In the context of the 'magnetars', highly magnetized NSs (dipole field strength on surface 10^{14-15} G; see Woods & Thompson 2004, for a review), it would certainly be useful to know how much magnetic flux and energy could be 'hidden' in the interior of the star. These stars undergo soft-γ-ray outbursts, releasing as much as 2×10^{46} erg of magnetic energy in less than a second. A field of 3×10^{14} G, if it fills the interior of the star, contains 2×10^{46} erg, and since these stars appear to have a lifetime of $\sim 10^4$ yr and to undergo large outbursts perhaps once a century, it seems likely that the average field strength in the interior is significantly greater than that on the surface.

Another way in which the poloidal/toroidal ratio may manifest itself is through its effect on the star's shape and moment of inertia. It has been known for some time (e.g. Chandrasekhar & Fermi 1953; Wentzel 1961) that a poloidal field will make a star oblate and a toroidal field prolate, and obviously with a mixed poloidal–toroidal field it will depend on the ratio of the two. In general, such a deformed star should undergo torque-free precession[2]; there is already some observational evidence for this (Cutler, Ushomirsky & Link 2003; Wasserman 2003; Akgün, Link & Wasserman 2006). If this precession is damped, then kinetic energy is minimized while conserving angular momentum and a prolate star will tend towards the alignment of its rotation and magnetic axes; while in an oblate star, the angle between the two axes will tend to 90°. In an Ap star, this damping process may or may not take on the order of a main-sequence lifetime (Mestel et al. 1981) but in a NS it may be much faster and a predominantly toroidal field in a fast-rotating NS could lead to strong emission of gravitational radiation. These effects of the magnetic field on a star's moment of inertia will be looked at in more detail in a forthcoming paper (Braithwaite & Nissanke, in preparation).

In Section 2, the instability in toroidal fields is described and some predictions are made about the stability of mixed poloidal–toroidal fields, and the properties of instability in poloidal fields are reviewed. In Section 3, analytic conditions are used to examine the stability of fields produced in simulations, and simulations are presented of the decay or otherwise of fields with various toroidal–poloidal ratios. I conclude, and discuss the results and their applications in Section 4.

2 INSTABILITY IN AXISYMMETRIC FIELDS: ANALYTIC RESULTS

In this section, I review the nature and properties of instability in purely toroidal and toroidal magnetic fields in stars, as well as look

[2] Purists may prefer the term 'nutation', although 'precession' occurs more frequently in the literature.

at stabilization of a predominantly toroidal field through the addition of a weak poloidal component and vice versa.

2.1 The Tayler instability

The stability of purely toroidal fields in stars was examined by Tayler (1973), who used the energy method of Bernstein et al. (1958) to derive necessary and sufficient stability conditions. Given a perturbation of the form

$$\xi \sim f(\theta)\mathrm{e}^{\mathrm{i}(nr+m\phi)+\sigma t}, \tag{1}$$

in spherical polar coordinates (r, ϕ, θ), he found that the stability conditions for $m \geq 2$ are less strict than for $m = 1$, so that if the goal is simply to distinguish between unstable and stable field configurations, these higher azimuthal wavenumbers need not be considered. The unstable modes can therefore be thought of as local in the meridional plane but global in the azimuthal direction.

2.1.1 Necessary and sufficient stability conditions

For stability against the $m = 0$ mode, we need the change in potential energy, as given by the following integral, to be positive for an arbitrary displacement field $\boldsymbol{\xi}$. In cylindrical coordinates (ϖ, ϕ, z):

$$\delta W \propto \int \varpi \, \mathrm{d}\varpi \, \mathrm{d}z \left\{ (.....)^2 + a\xi_z^2 + b\xi_z\xi_\varpi + c\xi_\varpi^2 \right\}, \tag{2}$$

where $(.....)^2$ is some function of $\boldsymbol{\xi}$ which is positive definite, and where

$$a = g_z \frac{\partial \rho}{\partial z} - \frac{\rho^2 g_z^2}{B_\phi^2 + \gamma P}, \tag{3}$$

$$b = g_\varpi \frac{\partial \rho}{\partial z} + g_z \frac{\partial \rho}{\partial \varpi} - \frac{2\rho g_z \left(\rho g_\varpi - 2B_\phi^2/\varpi \right)}{B_\phi^2 + \gamma P} - \frac{2B_\phi}{\varpi} \frac{\partial B_\phi}{\partial z}, \tag{4}$$

$$c = g_\varpi \frac{\partial \rho}{\partial \varpi} - \frac{\left(\rho g_\varpi - 2B_\phi^2/\varpi \right)^2}{B_\phi^2 + \gamma P} - \frac{2B_\phi}{\varpi} \frac{\partial B_\phi}{\partial \varpi} + \frac{2B_\phi^2}{\varpi^2}. \tag{5}$$

For δW to be positive, clearly it is sufficient (and can also be shown to be necessary) that the quadratic form is positive everywhere in the volume of integration. So, the stability conditions are that

$$a > 0\,, \quad c > 0 \quad \text{and} \quad b^2 < 4ac \tag{6}$$

everywhere in the (ϖ, z) plane in the star.

For stability against the $m = 1$ mode, we have a similar integrand consisting of one positive term and a quadratic where

$$a = g_\varpi \frac{\partial \rho}{\partial \varpi} - \frac{\rho^2 g_\varpi^2}{\gamma P} - \frac{B_\phi^2}{\varpi^2} - \frac{2B_\phi}{\varpi} \frac{\partial B_\phi}{\partial \varpi}, \tag{7}$$

$$b = g_\varpi \frac{\partial \rho}{\partial z} + g_z \frac{\partial \rho}{\partial \varpi} - \frac{2\rho^2 g_\varpi g_z}{B_\phi^2 + \gamma P} - \frac{2B_\phi}{\varpi} \frac{\partial B_\phi}{\partial z}, \tag{8}$$

$$c = g_z \frac{\partial \rho}{\partial z} - \frac{\rho^2 g_z^2}{\gamma P} + \frac{B_\phi^2}{\varpi^2}. \tag{9}$$

Tayler went on to show that it is impossible to satisfy all six of these conditions everywhere in the star, concluding that a stable equilibrium cannot be purely toroidal.

A hand-waving explanation of the instability mechanism is as follows. One can imagine the toroidal field as a stack of field rings which exert pressure on one another. Magnetic tension ('hoop stress') and external pressure prevents the discs from simply expanding outwards and thus relieving this pressure, but it is energetically favourable for the rings to slip sideways out of the equilibrium position, rather like the way an overloaded spinal column can result in a 'slipped disc'. The result is an $m = 1$ 'kink' mode, as illustrated in Fig. 2.

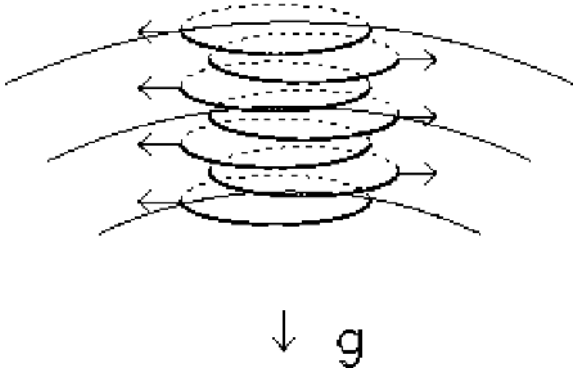

Figure 2. The form of the instability in a toroidal field near the axis of symmetry of a star. The $m = 1$ mode sets in before $m = 0$ and $m \geq 2$. (Figure from Spruit 1999.)

2.1.2 Unstable wavelengths and the stabilizing effect of an added poloidal field

The growth rate of the instability can be shown to be (Tayler 1957)

$$\sigma \sim \omega_\mathrm{A} \equiv \frac{v_\mathrm{A}}{r \sin\theta} = \frac{B_\phi}{r \sin\theta \sqrt{\rho}}. \tag{10}$$

In the case of an unstratified medium with infinite conductivity and zero kinetic viscosity, all vertical wavelengths (i.e. all n) are unstable. However, finite conductivity damps the highest n modes faster than they can grow, resulting in a maximum unstable n. Conversely, stable stratification restricts the growth of the lowest wavenumbers. This is because, as we see from the continuity equation, the instability results in vertical motions of the order of $\xi_\mathrm{r} \sim \xi_\mathrm{h} l_\mathrm{r}/l_\mathrm{h}$, where ξ_r and ξ_h are the displacements in the vertical (radial) and horizontal directions, respectively, and l_r and l_h are the length-scales in the vertical and horizontal, so that $l_\mathrm{r} = 1/n$. The horizontal instability force per unit mass pushing a fluid element away from its equilibrium position is $F_\mathrm{h} = \sigma^2 \xi_\mathrm{h}$, and the vertical buoyancy force pushing the fluid element back to equilibrium is $F_\mathrm{r} = N^2 \xi_\mathrm{r}$, where N is the buoyancy frequency. If the instability is to grow, we need therefore to have $\xi_\mathrm{h} F_\mathrm{h} > \xi_\mathrm{r} F_\mathrm{r}$. Now combining these two limits we have the following range of unstable wavelengths (Spruit 1999):

$$\sqrt{\frac{\sigma}{\eta}} > n > \frac{N}{l_\mathrm{h}\sigma}, \tag{11}$$

where η is the magnetic diffusivity. A toroidal field is stabilized if the left-hand side is less than the right-hand side. These wavelength limits were confirmed numerically by Braithwaite (2006).

Adding a radial field component B_r will also help to stabilize a toroidal field, as the horizontal displacements produced by the instability will bend the radial field lines, producing a restoring force. Using similar arguments to those in the previous paragraph, we can predict what field strength will be required for stabilization. The (horizontal) restoring force per unit mass is $\xi_\mathrm{h} B_\mathrm{r}^2/(l_\mathrm{r}^2 \rho)$ and, equating this to the force from the instability, we have instability if

$$\frac{\sigma\sqrt{\rho}}{B_\mathrm{r}} \sim \frac{B_\phi}{r \sin\theta \, B_\mathrm{r}} > n \tag{12}$$

using equation (10). This corresponds to a result in the case of an unstratified plasma from the unstable modes and dispersion-relation method (Tayler 1957).

Taking numbers typical for a main-sequence star (in cgs units) $r \sin\theta \sim 10^{11}$, $\rho \sim 1$, $B_\mathrm{r} \sim B_\phi \sim 10^3$ and $\eta \sim 10^2$, the term on the left-hand side of equation (11) turns out to be 10^6 times greater than that in equation (12). Similarly high ratios are found in WDs and NSs. This means that we can expect the stabilizing effect of the poloidal field to dominate over that of magnetic diffusion. Therefore, ignoring magnetic diffusion and combining the effects of stable stratification and poloidal field, we have stability if

$$\sigma^2 - \frac{N^2}{n^2 l_\mathrm{h}^2} - \frac{B_\mathrm{r}^2 n^2}{\rho} < 0, \tag{13}$$

which is true for all wavenumbers n if

$$\frac{B_\phi^4}{\varpi^4} < \frac{4 B_\mathrm{r}^2 \rho N^2}{l_\mathrm{h}^2}, \tag{14}$$

which can be rewritten in terms of the Alfvén frequency $\omega_\mathrm{A} \equiv B_\phi/(\varpi\sqrt{\rho})$ as

$$\frac{\omega_\mathrm{A}}{N}\frac{l_\mathrm{h}}{2\varpi} < \frac{B_r}{B_\phi}. \tag{15}$$

The second part of the left hand side will be roughly unity, so it is clear that the critical B_r/B_ϕ depends on the field strength in the star. In a main-sequence star, we have $\omega_\mathrm{A}^2/N^2 \sim E/U$, the ratio of magnetic to thermal energies; in neutron stars the buoyancy is weaker (Reisenegger 2008), so that $\omega_\mathrm{A}^2/N^2 \sim 10^2 E/U$. However, we expect $E/U < 10^{-6}$ in a real star, so a relatively weak poloidal field should be sufficient for stabilisation in any kind of star.

2.2 Instability of poloidal fields

It is known that not only purely toroidal fields, but also purely poloidal fields are also unstable (Markey & Tayler 1973; Braithwaite 2007). The instability begins in the region of the neutral line, the line where the poloidal component goes to zero. This instability is not unlike that in a toroidal field near the axis of symmetry – the poloidal field increases in proportion to distance from the neutral line and it is the pressure in the direction parallel to this line, which the 'loops' are exerting on each other, which drives the instability. The direction of the stratification is the important difference between the two instabilities; displacements must be approximately perpendicular to gravity, which in the poloidal case means that the loops move in a direction parallel to the star's axis of symmetry. This is illustrated in Fig. 3. The growth rate of this instability is calculated in the same way as in the toroidal case, so it is given by the local Alfvén frequency around the neutral line $\omega_\mathrm{A} \equiv B_\mathrm{p}/(s\sqrt{\rho})$, where s is the distance from the neutral line. Adding a toroidal component (i.e. a component parallel to the neutral line) can stabilize the field, since the instability increases the length of the neutral line, thereby stretching the toroidal field line lying on it. The higher azimuthal wavenumbers are stabilized first, so that the $m = 2$ wavenumber is the first to become unstable as the strength of the toroidal component is reduced. (Note that the $m = 0$ and 1 modes are prevented by conservation of momentum and angular momentum, respectively.) In Paper II, it was found that as an axisymmetric configuration diffuses outwards towards the stellar surface, the toroidal component is lost into the atmosphere, weakening it relative to the poloidal component, and eventually the $m = 2$ mode appears and the configuration evolves quasi-statically along a non-axisymmetric sequence. The minimum-energy state

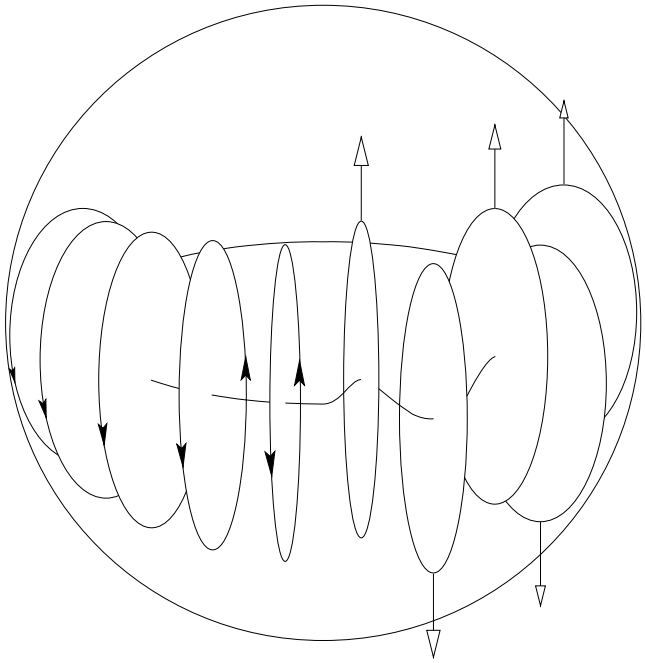

Figure 3. The form of the instability in a purely poloidal configuration. The left-hand side shows the equilibrium and the right-hand side the growth of a mode of particular azimuthal wavenumber.

of this non-axisymmetric equilibrium has comparable toroidal and poloidal components, which strongly suggests that an axisymmetric equilibrium cannot have a much stronger poloidal component than toroidal. A poloidal component which is stronger by some factor of order unity is possible, and the next section examines how large that factor can be. Note that this signals an asymmetry between the toroidal and poloidal cases, as there is no equivalent factor-of-order-unity argument giving an upper bound to the relative strength of the toroidal component.

The strength of toroidal field required for stabilization can be estimated with an analogous method to that described in Section 2.1.2, taking the wavelength to be $2\pi r_\mathrm{n}/m$ and arriving at the following stability condition:

$$\frac{B_\mathrm{p}}{s B_\mathrm{t}} < \frac{m}{r_\mathrm{n}}, \tag{16}$$

where s is the distance from the neutral line and r_m is the radius of the neutral line. Note that B_p is proportional to s in the neighbourhood of the neutral line. Although this stability condition should be taken as rather approximate since curvature and other effects have been ignored, it shows again that stability against the (most unstable) $m = 2$ mode requires the toroidal component to be at least comparable in strength to the poloidal component. Wright (1973) arrived at a similar stability condition (his equation 39):

$$0.24 B_\mathrm{p}(s_0) < B_\mathrm{t}, \tag{17}$$

where s_0 is some distance from the neutral line whose value is uncertain.

2.3 The effect of rotation

In the previous sections, the rotation of the star was not taken into consideration, but we may now look at its possible effect. First of all, we expect it to have an effect only in the 'fast'-rotating regime, i.e. when the rotation speed is faster than the Alfvén speed (Frieman

& Rotenberg 1960). Applying this condition to real astrophysical objects, we see some fast and slow rotators. We find the ratio of the magnetic and rotation time-scales to be

$$\frac{\Omega}{\omega_{\rm A}} = \frac{2\pi}{P\bar{B}}\sqrt{\frac{3M}{R}}, \tag{18}$$

where P is the rotation period, $\bar{B}$ is some average magnetic field in the interior of the star, and M and R are the stellar mass and radius. For $3\,{\rm M}_\odot$ MS stars, $0.8\,{\rm M}_\odot$ WDs and $1.4\,{\rm M}_\odot$ NSs, the numbers are

$$\frac{\Omega}{\omega_{\rm A}} \approx 3800 P_{10{\rm d}}^{-1} B_{5\,{\rm kG}}^{-1} \;\; \text{or} \;\; 18 P_{1{\rm d}}^{-1} B_7^{-1} \;\; \text{or} \;\; 0.05 P_{10\,{\rm s}}^{-1} B_{15}^{-1}, \tag{19}$$

where the periods are in units of 10 d, 1 d, 10 s and the field strengths 5 kG, 10 MG and 10^{15} G – typical values for magnetic MS stars, WDs and NSs (magnetars), respectively. Evidently the typical Ap star is in the fast-rotating regime; however, there are a few known examples with comparable field strengths but rotation periods of 30–100 yr and above, just putting them into the slowly rotating regime (Mathys 2008). There is also much variation amongst the magnetic WDs: a group exists with $P \sim 100$ yr and $B \sim 300$ MG while some others have $P \sim$ few hours and $B \sim 1$ MG (Ferrario & Wickramasinghe 2005), so this class of star contains both fast and (very) slow rotators. The magnetars show much less variation and all are slow rotators; the radio pulsars on the other hand are fast rotators.

In the fast-rotating stars, the rotation will certainly have some effect on the growth rate of any instability. In the rotating frame, the Coriolis force acts perpendicularly to any unstable displacement, giving rise to epicycles; in the absence of any diffusive mechanisms, this causes the fluid elements to come back to their original positions and stabilization results. This has been seen in simulations of the instability in a toroidal field (Braithwaite 2006). Diffusion though damps the epicycles and the instability returns, albeit with the growth rate reduced by some factor $\Omega/\omega_{\rm A}$ (Pitts & Tayler 1986; Spruit 1999). In the case of a strong poloidal field, a similar effect has been seen in simulations (Braithwaite 2007). It seems likely then that rotation does not affect the upper and lower bounds on $E_{\rm p}/E$.

3 STABILITY OF THE AXISYMMETRIC FIELD CONFIGURATIONS: NUMERICAL METHODS

Having derived some stability criteria for a mixed poloidal–toroidal field, it remains to see what this means for the stability of a global magnetic field configuration. Clearly, a globally stable configuration needs to be locally stable against the Tayler instability at each point in the star, as well as being stable in the neighbourhood of the neutral line. There are two obvious ways to proceed. The first is to find a global configuration and then check that a local analysis predicts stability at every location in the star for both types of instability. The second way is to construct a global configuration and then numerically follow its evolution in time.

3.1 Constructing an axisymmetric field

The basis for constructing axisymmetric field configurations whose stability we can probe will be the result of numerical simulations similar to those performed in Paper I, to where the reader is referred for a fuller account of the setup of the model; a brief outline is given here.

The code used is the STAGGER code (Nordlund & Galsgaard 1995; Gudiksen & Nordlund 2005), a high-order finite-difference Cartesian magnetohydrodynamics (MHD) code which uses a 'hyper-diffusion' scheme, a system whereby diffusivities are scaled with the length-scales presents so that badly resolved structure near the Nyquist spatial frequency is damped whilst preserving well-resolved structure on longer length-scales. This and the high-order spatial interpolation and derivatives (sixth order) and time-stepping (third order) increase efficiency by giving a low-effective diffusivity at modest resolution (128^3 here). The code includes Ohmic and well as thermal and kinetic diffusion. Using Cartesian coordinates avoids problems with singularities and simplifies the boundary conditions: periodic boundaries are used here.

The simulations model the star as a self-gravitating ball of ideal gas ($\gamma = 5/3$) of radius R in hydrostatic equilibrium with radial density and pressure profiles obeying the polytrope relation $P \propto \rho^{1+\frac{1}{n}}$, with the index n set to 3 here, since this gives stable stratification and is a reasonable approximation to an upper main-sequence star. It seems unlikely that a different EOS, for instance that of a NS, will make even much quantitative difference to the results. The important point is the stable stratification – the issue of magnetic equilibria in a non-stably stratified star will be explored in a forthcoming paper.

A boundary between the star and the surrounding volume is produced in the following way. In reality, we expect the field outside the star to be not only force-free (as is the usual approximation when looking at magnetic loops in the solar corona) but also curl-free, since a very tenuous medium will not sustain long-lived currents. Numerically, a potential (i.e. current-free) field is tricky to produce, but fortunately the same effect can be produced by adding a high magnetic diffusivity to the volume outside the star, and in practice the diffusivity chosen is the maximum allowed without having to reduce the time-step. This causes the field outside the star to relax fairly rapidly to a curl-free configuration. Also, the gas outside the star is hot, increasing the scaleheight and thus stopping the density from falling to greatly towards the edges of the computational box, preventing high Alfvén speeds and the lower time-step they would cause. The star is given an initially random magnetic field containing energy at all length-scales down to a limit of a few grid spacings, and the MHD equations are integrated in time to follow the evolution of the field. Within a few Alfvén crossing times, a stable equilibrium is reached. In the case where the field is less centrally concentrated, the equilibrium is non-axisymmetric, consisting of twisted flux tubes meandering at roughly constant depth under the surface of the star. This case was examined in detail in Paper II. In the case of more centrally concentrated (i.e. deeply buried) initial fields, an approximately axisymmetric field forms. Ignoring the small deviations from axisymmetry, there appear to be two basic degrees of freedom:[3] the concentration of the field into the centre of the star, which can be parametrized as $r_{\rm n}$, the distance between the axis of symmetry and the neutral line, and the poloidal fraction of total energy $E_{\rm p}/E$. In this two-dimensional parameter space lies an area of stability through which the star slowly moves in time, as a result of diffusive processes such as finite conductivity, to ever increasing $r_{\rm n}$ and the eventual end of its stable axisymmetric life, as described above and in Paper II. It is the aim here to find the boundaries of that area of stability.

The first step is to produce a stable field in a simulation (i.e. run with arbitrary initial conditions for a few Alfvén crossing times until the field has settled down into an equilibrium) and axisymmetrize it,

[3] There are other, more subtle degrees of freedom concerning the exact shape of the field lines, but they appear to be less important, and are beyond the scope of this study.

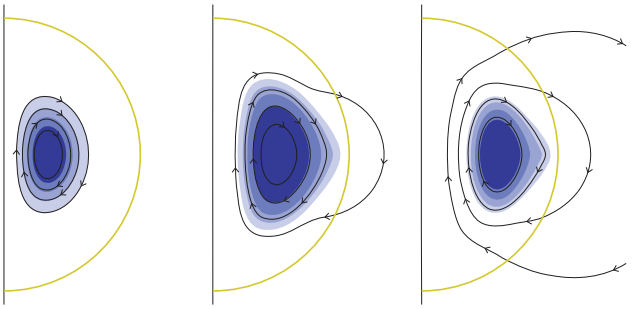

Figure 4. Projection on to the meridional plane of the stable magnetic field configurations with $r_n/R = 0.33$, 0.47 and 0.58. The yellow semicircle is the surface of the star, and the black lines and blue shading represent the poloidal and toroidal components of the field, respectively. The contours of the toroidal part are actually contours of $\varpi\ B_\phi$; it is clear that this quantity is roughly constant on poloidal field lines. The poloidal lines plotted are separated by equal quantities of poloidal flux.

using an axis defined by $\int \boldsymbol{r} \times \boldsymbol{B}\, \mathrm{d}V$. Although the fields produced in the simulations are already approximately axisymmetric, perfect axisymmetry simplifies the stability analysis. Also, the small asymmetry between the two hemispheres is removed so that the field is symmetrical about the $z = 0$ plane. Now, this symmetrized star can be put back into the simulation and evolved in time (the 'fiducial simulation'), where it slowly diffuses outwards, the value of r_n rising as it does so. Its stability can then be examined at various points along this diffusive evolution track, both analytically, using the methods described in Section 2, and numerically, by changing the relative strengths of the poloidal and toroidal parts and using that as the initial conditions for a new simulation. In this way, the boundaries of the stable area in r_n–E_p/E parameter space can be found. In Fig. 4, we see the axisymmetric field at the times $t/\tau_A = 5.2$, 69.7 and 97.0 when $r_n/R = 0.33$, 0.47 and 0.58. Time is measured in units of the Alfvén crossing time, defined here as $\tau_A \equiv R\sqrt{M/2E}$ where E is the total magnetic energy and M is the mass of the star. Note that it can be seen in the figure that the contours of ϖB_ϕ are parallel to the poloidal field lines. This result can be derived analytically (Mestel 1961; Roxburgh 1966) from $\nabla \cdot \boldsymbol{B} = 0$ and from the recognition that the azimuthal component of the Lorentz force must be zero everywhere because in an axisymmetric equilibrium it cannot be balanced by gravity $\rho \boldsymbol{g}$ or the pressure gradient $-\nabla P$.

In Fig. 5, are plotted various quantities from the fiducial run which change in time as the magnetic field evolves diffusively: the neutral line radius r_n, the poloidal energy fraction E_p/E and the fraction of the poloidal flux which breaches the surface of the star Φ_{surf}/Φ_p.

First, the case where the toroidal field dominates will be examined, and then in Section 3.3 the poloidal-dominated case is looked at, in order to find both boundaries of stability, i.e. both upper and lower bounds to E_p/E.

3.2 Stability of a predominantly toroidal field

In this section, I examine the stability of fields with low E_p/E, firstly with a combination of Tayler's stability conditions and equation (14), and secondly with simulations using different values of E_p/E as initial conditions.

3.2.1 Analytic stability conditions

The $m \geq 2$ modes always set in after the $m = 1$ mode and need not be considered here. Taking the output of the fiducial simulation,

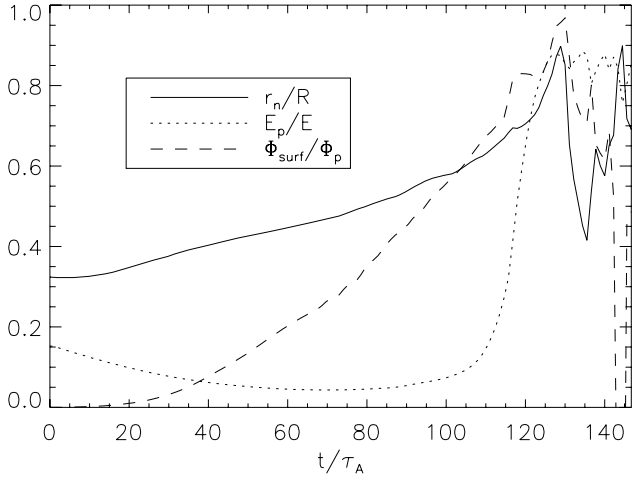

Figure 5. The neutral line radius r_n, the poloidal energy fraction E_p/E and the fraction of poloidal flux which breaches the surface of the star Φ_{surf}/Φ_p against time (in units of the Alfvén crossing time). Transition to non-axisymmetric equilibrium occurs at around $t/\tau_A = 120$.

described in the previous section, I apply Tayler's six conditions (equation 6) for both $m = 0$ and 1 modes to the toroidal component of the field, at the three points in time shown in Fig. 4. Looking at where in the star the conditions are met, the first result is that the first two conditions, $a > 0$ and $c > 0$, for both the $m = 0$ and 1 modes are satisfied everywhere in the star at all points in time. In

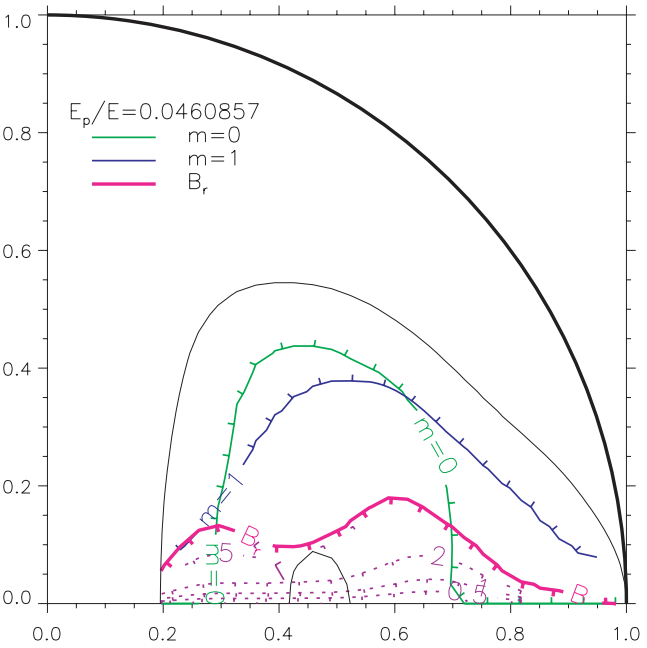

Figure 6. Half of the meridional plane (the other half being identical) with $r_n/R = 0.47$ value. The thick black line is the surface of the star and the thin black lines are two selected poloidal field lines, showing the locations of the 'closed' poloidal region (where the toroidal field resides) and neutral line. The regions stable against the $m = 0$ and 1 even in the absence of a poloidal field are illustrated by the green and blue lines; the ticks point into the region of instability. The thick pink line shows which area is stabilized by the radial component of the field B_r. Dotted and dashed purple lines are contours of minimum and maximum unstable wavelengths, in units of the grid spacing $\mathrm{d}x \approx 0.03R$, as calculated by solving for n in equation (13) and taking $\lambda = 2\pi/n$.

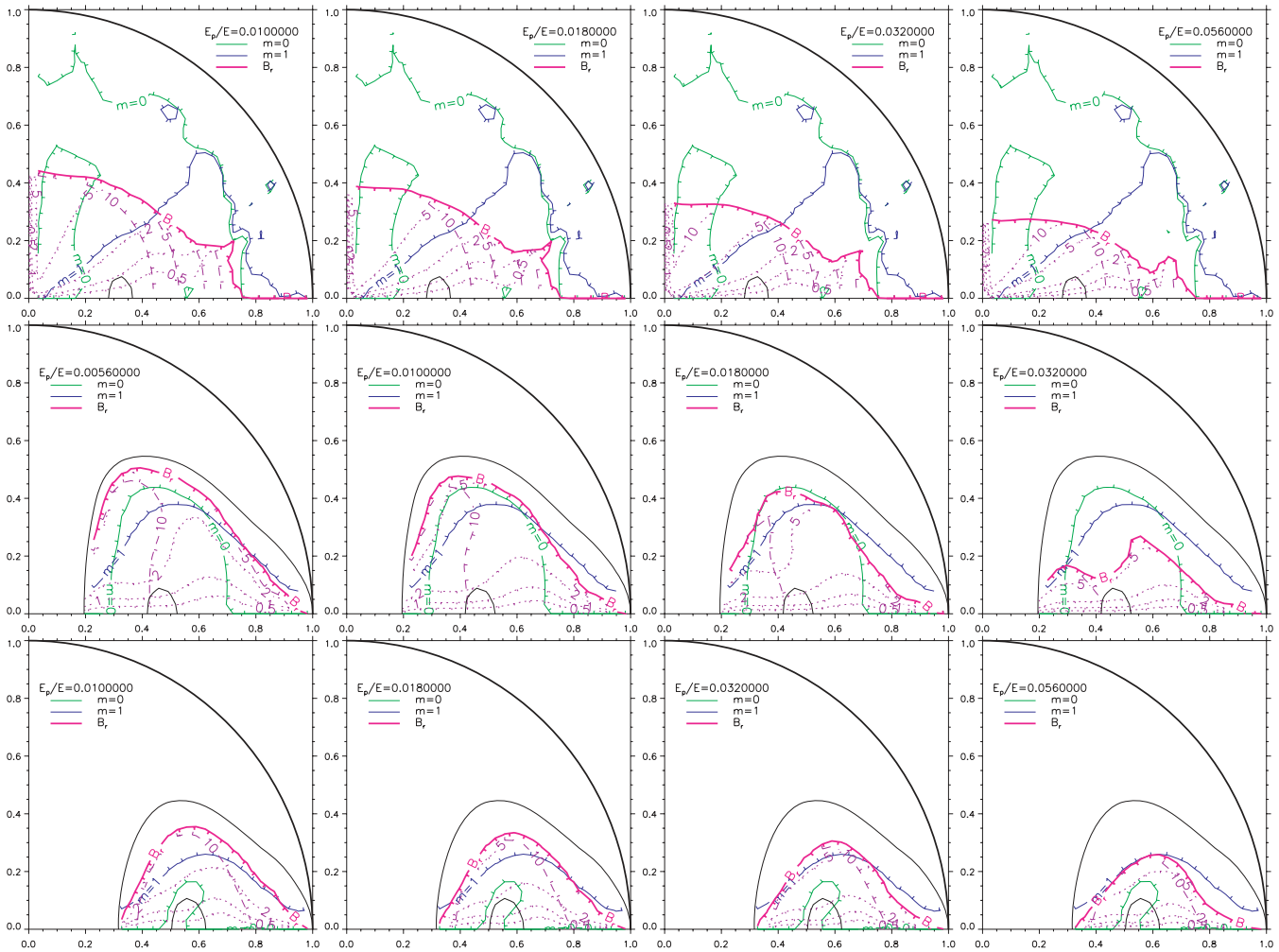

Figure 7. Stability lines for various values of $E_p/E = 0.01$ at three points in the fiducial simulation with $E/U = 1/400$. Top row: $r_n = 0.33R$ and $E_p/E = 0.01$, 0.018, 0.032 and 0.056; middle row: $r_n = 0.47R$ and $E_p/E = 0.0056$, 0.01, 0.018 and 0.032; bottom row: $r_n = 0.58R$ and $E_p/E = 0.01$, 0.018, 0.032 and 0.056. See Fig. 6 for an explanation of the various lines plotted.

contrast, the two $b^2 < 4ac$ conditions are not met everywhere; the regions in the meridional plane where they are and are not satisfied this are plotted in Fig. 6, for the case where $r_n = 0.47R$. Of course, this is the conclusion that Tayler arrived at – that a purely toroidal field is always unstable in at least some part of the star. The field which forms in the simulations is stable against the Tayler instability only because of the presence of the poloidal component. However, it is possible that the toroidal component can be stabilized with a weaker poloidal component than is actually present in the fiducial simulation. We can use equation (14) to estimate what strength the poloidal field needs to be at any particular point, so an estimate for the minimum overall strength of the poloidal component is that at which this condition is just satisfied at every point where Tayler's criteria are not satisfied. It should be stressed, however, that this approach is only approximate, since we have ignored curvature effects, and also because l_h is undetermined – we will simply assume here that $l_h \sim R$. The area stabilized according to equation (14) is also plotted in Fig. 6. It is clear from the figure that the entire region unstable to $m = 1$ is stabilized by the poloidal field, as well as almost the entire region otherwise unstable to $m = 0$, but that two small regions are apparently still $m = 0$ unstable. However, looking at the minimum unstable wavelength given by equation (13), we see that both of these areas, there is barely space to fit one wavelength as $\lambda_{min} \sim 2\,dx \approx 0.06R$. This explains the stability in the simulations at this poloidal/toroidal ratio. Note that the reason for expressing the minimum and maximum unstable wavelengths in terms of the grid spacing is that we can easily check if the simulation is running at sufficiently high resolution – clearly, the wavelength needs to be at least a few grid spacings to be properly resolved.

If the relative strengths of the toroidal and poloidal components are now changed (while keeping the total energy E constant), the position of the B_r stabilization line changes.[4] Fig. 7 shows the positions of the stability lines at various ratios E_p/E of poloidal/total energy at the three different values of r_n.

Looking first at the top row of Fig. 7 ($r_n/R = 0.33$, $E_p/E = 0.139$ in the fiducial simulation), it can be seen that the $E_p/E = 0.01$ should be unstable, as there is an $m = 1$ unstable region on the left where the minimum unstable wavelength is only a few grid spacings, small enough to fit into the space available (but large enough to be resolved numerically in the simulations described below). However,

[4] In principle, the $m = 0$ and 1 stability lines also move, but in the case of strong toroidal field and constant total energy, the toroidal field strength changes only by a small factor and the lines move very little.

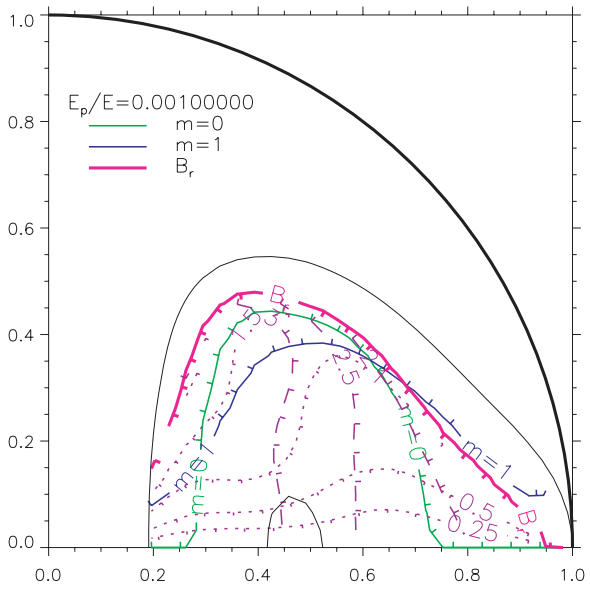

Figure 8. Stability lines for $r_n = 0.47\,R$ and $E_p/E = 0.001$ in the weak-field case ($E/U = 1/4000$). The resemblance with the $E_p/E = 0.01$, $E/U = 1/400$ plot in Fig. 7 is obvious. The only significant difference is that the unstable wavelengths are a factor $\sqrt{10}$ shorter in the weaker field case. See Fig. 6 for an explanation of the various lines plotted.

the minimum wavelength looks too high in the $m = 0$ unstable zone. The 0.018 case is more marginal but there may still be space to fit an unstable wavelength of five grid spacings ($0.15R_*$) into the $m = 1$ unstable space. The 0.032 case looks also marginal, but 0.056 does look stable. Therefore, the critical value of E_p/E is perhaps around 0.018 or 0.032. Repeating this analysis on the middle row of Fig. 7 ($r_n/R = 0.47$, $E_p/E = 0.046$ in the fiducial simulation), we get a stable E_p/E minimum at around $E_p/E = 0.0056$ to 0.01. Finally on the bottom row of Fig. 7 ($r_n/R = 0.58$, $E_p/E = 0.066$ in the fiducial simulation), we see that practically the entire region of interest is $m = 0$ unstable, which is stabilized by the poloidal field at around $E_p/E = 0.056$, but that the $m = 1$ mode should be stabilized at a somewhat lower poloidal energy ratio, perhaps at roughly 0.01.

These lower limits on E_p/E are, as discussed in Section 2.1.2, dependent on the absolute field strength which I parametrize as E/U, the ratio of magnetic to thermal energies. Changing the magnetic field energy in the fiducial simulation by a factor of 10 so that $E/U = 4000$ and repeating the exercise above results in stability at a value of E_p/E a factor of 10 lower, as can be seen in Fig. 8, where the ratios E_p/E and E/U are both a factor of 10 lower than in the second plot of the second row of Fig. 7, but the result is near-identical stability lines. The only significant difference between the two is that the unstable wavelengths are a factor $\sqrt{10}$ lower in the weaker field case.

3.2.2 *Simulations with different E_p/E*

To verify this assessment above, it is possible to use these altered E_p/E configurations as the initial conditions for simulations. I use here simulations with $E/U = 1/400$. First, the star is allowed to relax to equilibrium by keeping the magnetic field constant and letting the pressure field adjust until it balances the Lorentz force. After 10 or so sound crossing times, this relaxation has taken place. A small white-noise perturbation is then added to the density field, and the magnetic field is allowed to change, i.e. the induction equation is

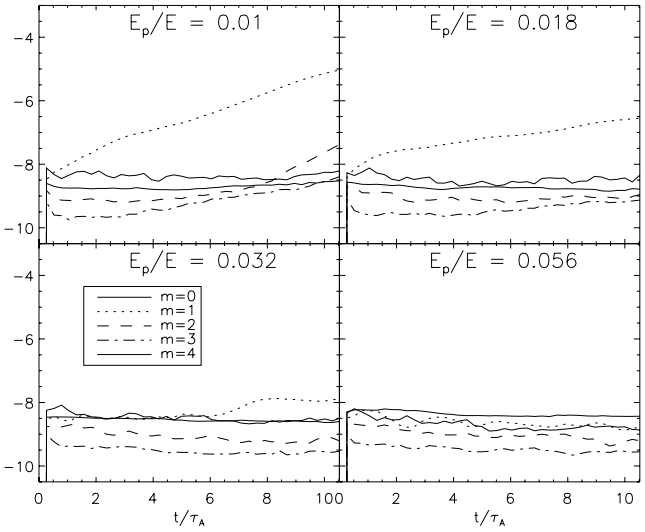

Figure 9. Log amplitudes of modes $0 \le m \le 4$ (solid, dotted, dashed, dot–dashed and dot–dot–dot–dashed, respectively) in simulations with $r_n/R = 0.33$ and $E_p/E = 0.01$, 0.018, 0.032 and 0.056. The stability threshold appears to be around 0.032, below which the $m = 1$ mode is the dominant mode.

switched on (this defines $t = 0$ in the following plots). In Fig. 9, the amplitudes of the azimuthal modes $m = 0$ to 4 (an rms integration over the meridional plane of velocity component v_θ) are plotted against time for simulations with the following values of E_p/E: 0.01, 0.018, 0.032 and 0.056, the initial conditions having been taken from the fiducial run at $r_n/R = 0.33$ before having the poloidal energy ratios changed by hand. It can be seen in the figure that the threshold is at $E_p/E \approx 0.032$.

This exercise was then repeated with the equilibria of different values of r_n/R: 0.47 and 0.58 (see Figs 10 and 11). The former is easy enough to interpret: the threshold is around $E_p/E = 0.01$. The small contamination we see in $m = 4$ from the geometry of the computational box is visible here but much greater in the $r_n/R = 0.58$ simulations, presumably because at higher r_n the field has a stronger interaction with the sides of the computational box. Here,

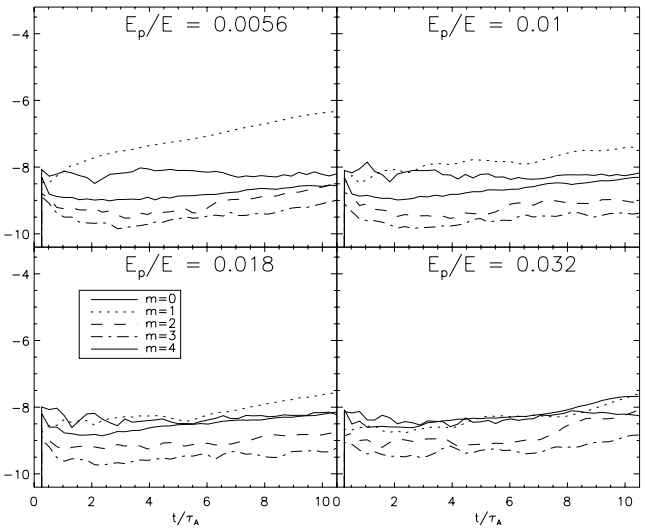

Figure 10. Log amplitudes of modes $0 \le m \le 4$ in simulations with $r_n/R = 0.47$ and $E_p/E = 0.0056$, 0.01, 0.018 and 0.032. The stability threshold appears to be around 0.01 or 0.018.

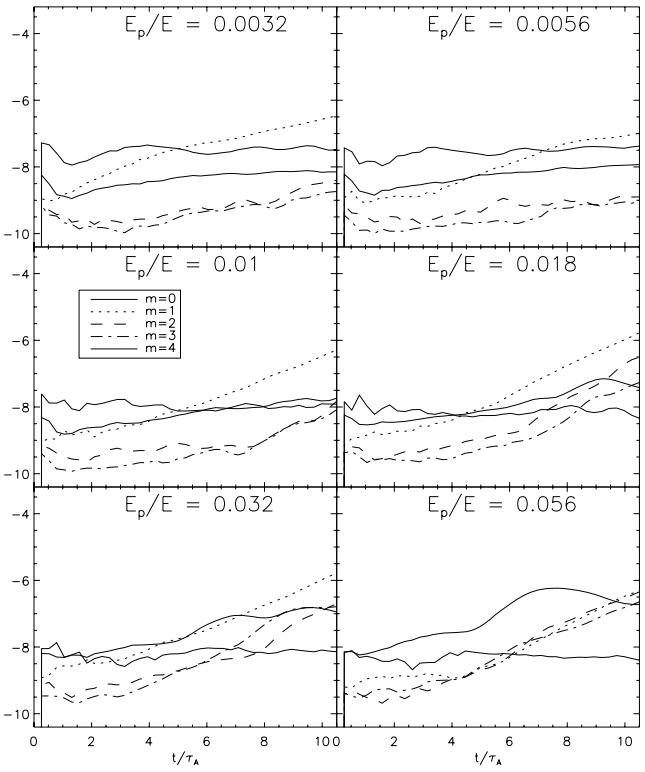

Figure 11. Log amplitudes of modes $0 \leq m \leq 4$ in simulations with $r_n/R = 0.58$ and $E_p/E = 0.0032$, 0.0056, 0.01, 0.018, 0.032 and 0.056. The $m = 0$ mode appears to be stable at all ratios considered here, whilst the $m = 1$ mode appears to stabilize at around $E_p/E = 0.056$ (see the text).

the ratio 0.056 simulation, which we know to be stable or almost so because the fiducial run has a ratio 0.066, has significant $m = 4$ contamination but we can see that the $m = 1$ mode is stable at least for the first few Alfvén crossing times, so it looks like the critical ratio is somewhere between 0.032 and 0.056. Surprisingly, the $m = 0$ mode seems stable at all ratios presented in the figure. This is at odds to the conclusions of Section 3.2.1, where we found that whilst $m = 1$ is stable above 0.01, the $m = 0$ mode should be unstable up to $E_p/E = 0.056$ or thereabouts. The reason for this discrepancy is not immediately clear, but may have something to do with effects ignored in this study such as curvature effects – the unstable region at this value of r_n is near the equator where these could be important.

At this juncture, it is necessary to look at the minimum and maximum wavelengths plotted in Fig. 7 to check that the simulations have sufficient resolution, as it is conceivable that a E_p/E ratio which is in reality unstable could appear to be stable in a simulation simply because the unstable wavelengths are too low to be resolved. Looking at the top row, where the $E_p/E = 0.032$ simulation is the first which appears stable, we see that the unstable region near the axis of symmetry has a maximum unstable wavelength of more than 10 grid spacings ($10\,\mathrm{d}x \approx 0.3R$, about the size of the unstable region) and a minimum wavelength of greater than $5\,\mathrm{d}x$. Now, in previous simulations (e.g. Braithwaite 2006), it was found that this high-order code can resolve modes of wavelength $8\,\mathrm{d}x$ almost perfectly, so it seems unlikely that a $\lambda \approx 5\,\mathrm{d}x$ mode is entirely suppressed. Looking at the middle and bottom rows, where the $E_p/E = 0.01$ and 0.032 simulations, respectively, are the first which appear stable in the simulations, the minimum wavelengths in the $m = 1$ unstable regions are also around $5\,\mathrm{d}x$ in both the cases.

Ideally one would now perform simulations with different field strengths, i.e. different values of E/U from the value 1/400 used above, in order to check the analytic prediction that the critical poloidal energy fraction $(E_p/E)_{crit} \propto E/U$. However, we see from Fig. 8 that the unstable wavelengths will be badly resolved or not resolved at all, and therefore that significantly higher numerical resolution would be required. At higher field strengths we are no longer in the physically interesting weak-field regime, as the structure of the star becomes significantly non-spherical. Checking this result numerically at the higher resolution required will be left for the future. It is not inconceivable of course that some other instability not considered here could become relevant at lower field strengths.

3.3 Stability of a predominantly poloidal field

We have seen that an axisymmetric configuration with much stronger a toroidal component than poloidal can be stable. However, we have a reason to believe that the opposite is not true; we expect that a field with a much stronger poloidal component will make a transition to non-axisymmetric equilibrium.

We can now apply the stability conditions (equations 16 and 17) to the fiducial simulation at the three points in time used in the previous section, i.e. when $r_n/R = 0.33$, 0.47 and 0.58. We find that the thresholds in E_p/E are 0.71, 0.48 and 0.69 using equation (16). How to calculate Wright's (1973) threshold is not obvious; one way is to look at the conditions near the neutral line and use $s_0\, B_p/s$ for $B_p(s_0)$ and set s_0 to r_n, and use the value of B_t on the neutral line. This gives thresholds of 0.91, 0.80 and 0.91. Wright points out that his stability condition is a necessary condition, and should be interpreted as a lower bound on the toroidal field required for stabilization.

To test the strength of toroidal field required for stabilization, simulations analogous to those presented in Section 3.2.2 were performed, this time with high values of E_p/E. The perturbation added in this case differs from the white noise used in the previous section: a large-scale perturbation was added to azimuthal modes $m = 2$ to 8. In Figs 12–14, the amplitudes of modes $m = 0$ to 4 are plotted against time for different poloidal energy ratios at different values of r_n.

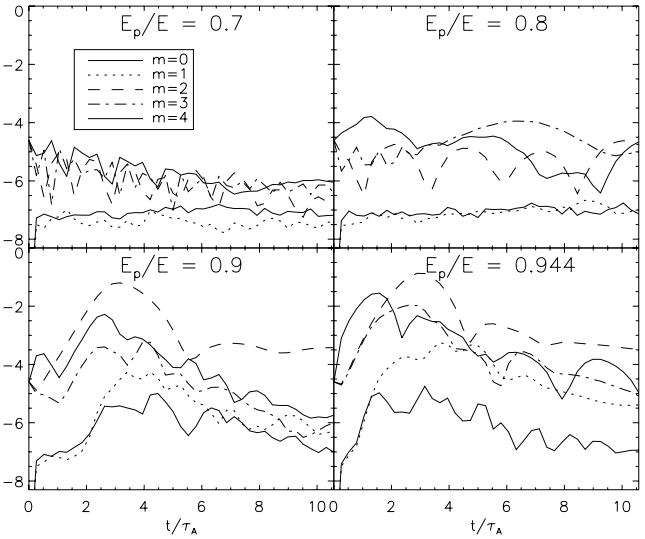

Figure 12. Log amplitudes of azimuthal modes $0 \leq m \leq 4$ (solid, dotted, dashed, dot–dashed and dot–dot–dot–dashed, respectively) in simulations with $r_n = 0.33R$. The stability threshold appears to be between 0.8 and 0.9.

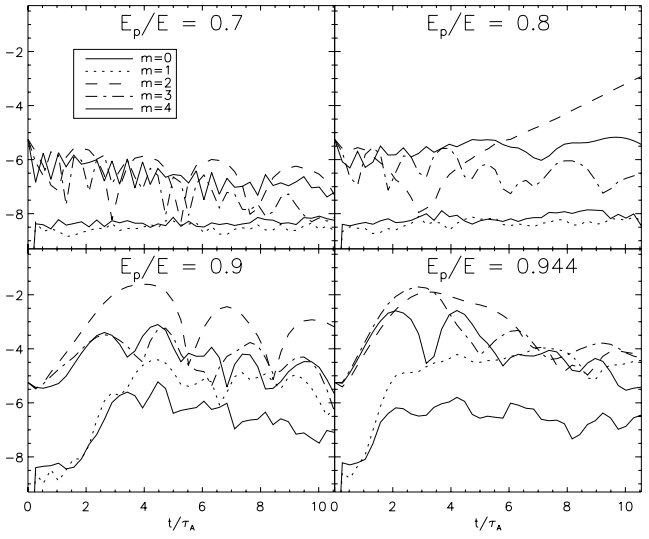

Figure 13. Log amplitudes of azimuthal modes $0 \leq m \leq 4$ in simulations with $r_\mathrm{n} = 0.47R$. The stability boundary is around 0.8.

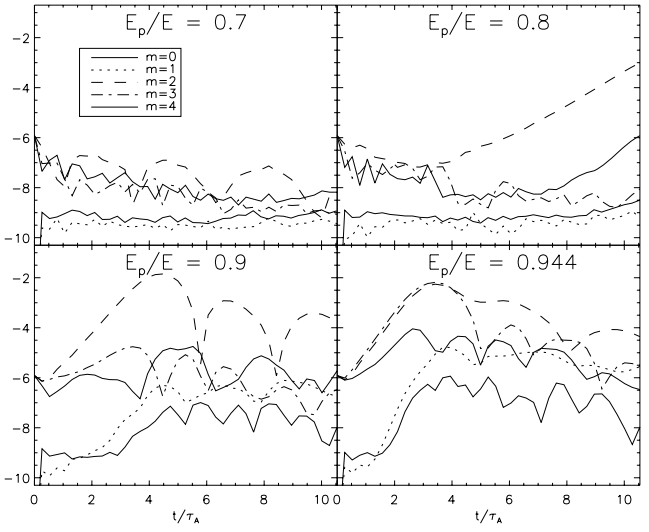

Figure 14. Log amplitudes of azimuthal modes $0 \leq m \leq 4$ in simulations with $r_\mathrm{n} = 0.58R$.

The thresholds in all the cases seem to be at $E_\mathrm{p}/E \approx 0.8$. In the $r_\mathrm{n} = 0.33R$ simulations (Fig. 12), at 0.8 (and at 0.7), an oscillatory behaviour can be seen in the $m = 2$ mode, indicating stability. At 0.9, the $m = 2$ mode is dominant; at 0.944, both $m = 2$ and 3 grow (the $m = 4$ mode is probably just numerical contamination at these ratios, but will become properly unstable above some threshold in E_p/E). Looking at Fig. 11, where $r_\mathrm{n} = 0.47R$, we see that $E_\mathrm{p}/E = 0.7$ is clearly stable; at 0.8, the $m = 2$ appears stable and then unstable – this is probably because the magnetic field is just below the threshold and is taken over it by continuing secular evolution, which weakens the toroidal component faster than the poloidal. It is visible in the plots that at higher poloidal energy ratios the higher azimuthal modes become unstable. Similarly, we see in Fig. 12 ($r_\mathrm{n} = 0.58R$) that the stability threshold is very close to 0.8. Very clear here is the stability (hence oscillations) of $m = 3$ at 0.9 but unstable growth at $E_\mathrm{p}/E = 0.944$. Of course, oscillations follow unstable growth when saturation, i.e. a new non-axisymmetric equilibrium, is reached.

A perhaps more elegant way to present the output from simulations is to plot a map of the field on the surface of the star. Figs 15 and 16 are such maps of B_r; all are taken from the $r_\mathrm{n}/R = 0.47$ simulations. Fig. 14 follows the evolution in time of three simulations with different E_p/E ratios; by the end of the simulations, new equilibria have been reached in the unstable cases. These maps confirm that $E_\mathrm{p}/E = 0.7$ is stable (apart from a small $m = 4$ numerical contamination), that 0.8 is stable at first and then succumbs to the $m = 2$ mode and that the 0.9 field is unstable mainly to the $m = 2$ mode and eventually finds its way into a new equilibrium. Fig. 16 shows the equilibria reached in simulations with even higher E_p/E ratios; evidently, the higher the ratio, the more complex the resulting equilibrium.

It seems then that a magnetic field becomes unstable as the poloidal energy fraction exceeds about 80 per cent, and this threshold depends only weakly on the central concentration of the field (i.e. on r_n). Just above this threshold, the only unstable mode is $m = 2$, which is reassuringly well resolved by simulations at this resolution. At higher values of E_p/E, higher modes become unstable, which is exactly what we expect because higher azimuthal modes have to do more work against the toroidal field, in proportion to the value of m. Therefore, the $m = 3$ mode becomes unstable with a toroidal field two-third the strength of that at the $m = 2$ stability threshold, so that if the $m = 2$ threshold is $E_\mathrm{p}/E \approx 0.8$, then the $m = 3$ threshold will be at $E_\mathrm{p}/E \approx 1 - (1–0.8)(2/3)^2 = 0.911$ (ignoring the small change in poloidal field strength resulting from the change in E_p/E at constant E). This can be seen for instance in Fig. 14 and confirms the m dependence of in equation (16).

The stability thresholds found from these simulations agree only qualitatively with the predictions (equations 16 and 17). This probably has to do with effects not included in the analysis, such as the toroidal geometry of the flux tube, the fact that the poloidal field lines are not circular in the neighbourhood of the neutral line – in fact they are decidedly elliptical, and the toroidal field falls off away from the neutral line.

It is informative to think about this evolution into a new equilibrium in terms of the magnetic helicity, defined as $\int \boldsymbol{B} \cdot \boldsymbol{A}\, \mathrm{d}V$, where $\boldsymbol{A}$ is the vector potential. As the field evolves on a dynamical time-scale, helicity is conserved and the field can be thought of as evolving into the lowest energy state for that value of helicity. Essentially, helicity can be thought of as the product of toroidal and poloidal fluxes, so that as we go to higher E_p/E ratios, the helicity falls, and below some threshold the lowest energy state is non-axisymmetric. The initial equilibrium is essentially a twisted flux tube lying in a circle around the equator of the star, and the transition to non-axisymmetric equilibrium is a matter simply of stretching this flux tube into a more complex arrangement. In the process of stretching the tube, the toroidal component (i.e. the component parallel to the axis of the tube, the neutral line) is amplified (since the tube becomes narrower) and the poloidal component becomes weaker, eventually bringing the two components to roughly equal strengths, because the energy minimum for a given helicity, i.e. for a given product of toroidal and poloidal field strengths, will have the two components roughly equal to each other. At higher E_p/E ratios therefore, more stretching is required to make the two components equal. This can be clearly seen in Fig. 16. Now in the case where $E_\mathrm{p}/E = 1$, the field has zero magnetic helicity and no amount of flux tube stretching can result in an equilibrium. However, there are diffusive processes at work which can either create helicity or split the one original flux tube into two or more tubes which can have helicity of different signs and which add up to zero, although it is likely that a lot of time will pass before any equilibrium is reached

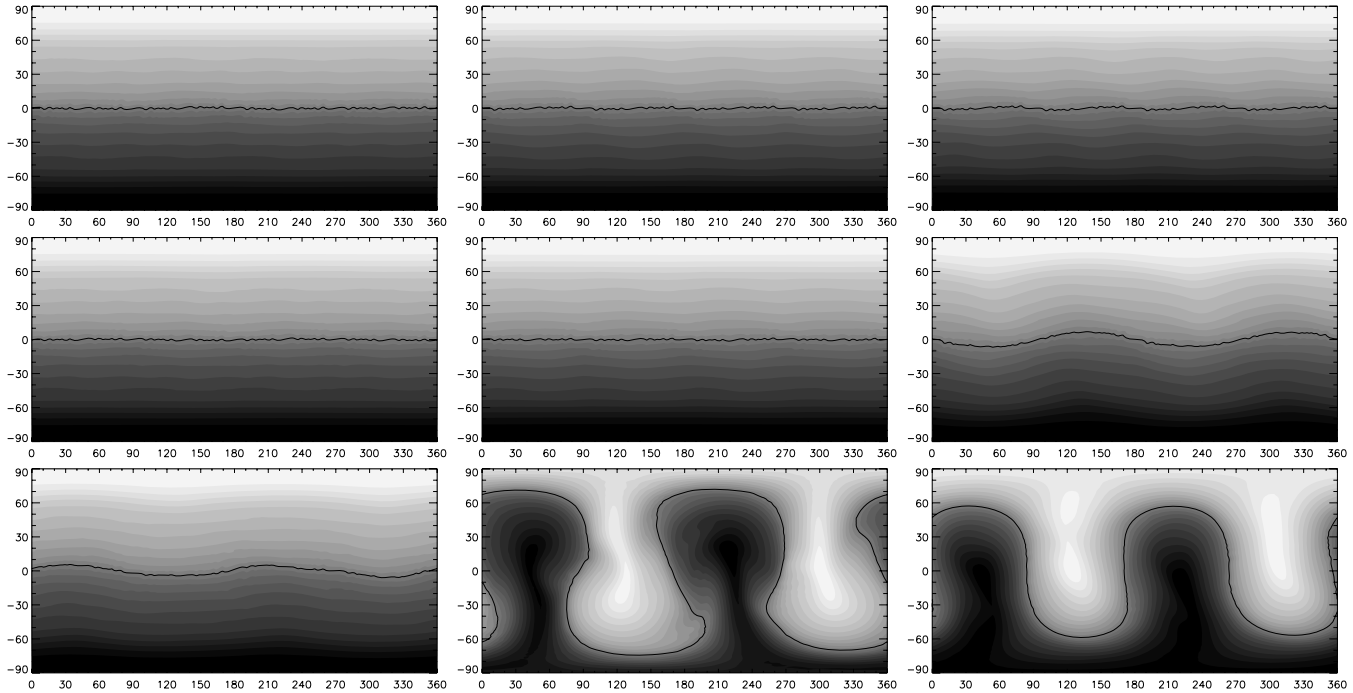

Figure 15. Behaviour of the magnetic field when the poloidal component is stronger than the toroidal, near the maximum poloidal/toroidal ratio. Maps of the radial magnetic field B_r on the stellar surface at three points in time ($t/\tau_A = 2.9$, 5.8 and 10.5; plates on the left-hand panel, middle panel and right-hand panel, respectively) of the simulations with $r_n/R = 0.47$ and $E_p/E = 0.7$, 0.8 and 0.9 (top, middle and bottom rows, respectively). White and black represent the strongest positive and negative B_r, and the black line shows the position of $B_r = 0$, which is initially at the equator. The simulation on the top row shows stability; on the middle row we see initial stability followed by an $m = 2$ mode and the simulation with $E_p/E = 0.9$ shows a strong growth of the $m = 2$ mode which then saturates after a few Alfvén crossing times as the field settles into a new equilibrium.

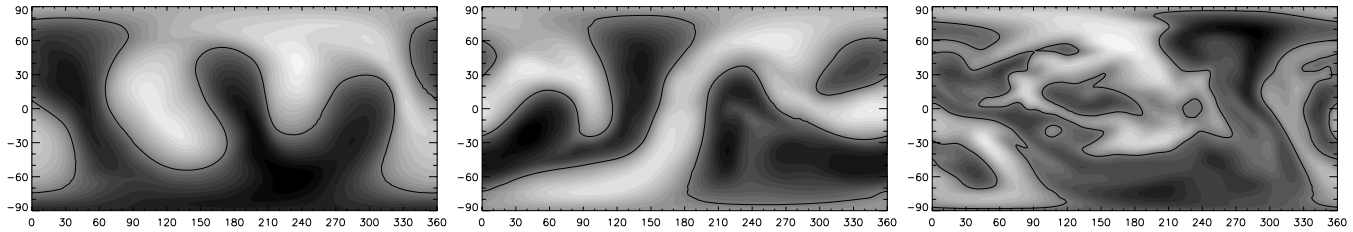

Figure 16. As Fig. 15 but all three B_r maps are at one point in time ($t/\tau_A = 10.5$) in three different simulations with $E_p/E = 0.968$, 0.99 and 1.0. Evidently, at higher initial E_p/E ratios, the non-axisymmetric equilibria reached are more complex.

and the energy of the equilibrium will be very much lower than the original energy.

4 CONCLUSIONS AND DISCUSSION

In this paper, I have looked at the lower and upper limits on the fraction of energy in the poloidal component of an axisymmetric magnetic field. To find these limits, I took the output from a simulation where a 'turbulent' initial magnetic field evolves into an axisymmetric equilibrium, changed the relative strengths of the poloidal and toroidal components by hand, and used that as the initial conditions for new simulations. This was supplemented with more analytic methods including the necessary and sufficient stability conditions found by Tayler (1973) (it is incidentally found that four of his six conditions are always met at every point in the star). The two methods are in broad agreement.

The result of this investigation is that while the upper limit on the poloidal energy fraction E_p/E is around 80 per cent, the lower limit depends on factors such as the radius of the neutral line r_n and can be between 1 per cent and roughly 5 per cent for a star constructed from a polytrope of index $n = 3$ (which approximates to an upper-main-sequence star) and where the ratio of magnetic to thermal energies $E/U = 1/400$. This lower limit is expected to be proportional to the ratio E/U, so that $(E_p/E)_{crit} \sim 10\,E/U$. These limits will also depend on other factors not explored here, such as the equation of state and density profile of the star (that used in the simulations approximates an upper main-sequence star), but these should not affect the results in more than a modest quantitative manner; however in a NS we might expect a lower limit of $(E_p/E)_{crit} \sim 10^3 E/U$. The upper limit found here broadly confirms what was expected from the analysis in Paper II and from the analyses of Wright (1973) and Markey & Tayler (1974), who found that the toroidal field must be at least about a quarter of the strength of the poloidal field. The lower limit on E_p/E had not been looked at before.

The question of what ratios we actually expect to find in nature has not yet been answered. It will depend on the state of the magnetic field left over from the convective protostellar phase (whether we are looking at main-sequence stars, WDs or NSs) and on the subsequent secular evolution. In the fiducial simulation described,

E_p/E does fall to around 0.046 and is below 0.1 for most of the period of diffusive evolution. Given that a star is generally strongly differentially rotating when it is formed, and that any seed field will be wound up and predominantly toroidal, it seems plausible that the eventual equilibrium could have rather low E_p/E. A proper study of the effect of initial conditions on the resulting equilibrium will be left for the future.

It remains to look at some of the implications of these results. The magnetic field of a star can have various effects on its appearance and behaviour. In upper main-sequence stars and WDs, we can directly observe the field on the surface via the Zeeman effect, and it turns out that many, if not most, do have roughly axisymmetric configurations. In NSs, we measure the spin-down and infer from that the dipole component on the surface. Below the surface of the star, there could be a deeply buried field (with low r_n and very low Φ_{surf}/Φ_p) and/or a very strong toroidal component, both of which could in effect 'hide' magnetic energy from view. This is of obvious interest in the study of magnetars, NSs with observed dipole fields of 10^{14-15} G whose emission in X rays and γ rays is powered by the decay of the magnetic field. The possibility that these stars could contain a large quantity of energy hidden from view could explain the large energy output of these objects. A field of 10^{15} G contains around 2×10^{47} erg in magnetic energy, and flare has been observed which emitted a tenth of that quantity in less than a second. According to the standard flare model, some slow evolution of the magnetic field in the core results in stress build-up in the crust, which eventually results in the crust cracking and a release of energy, but it is difficult to imagine this mechanism releasing a large fraction of the magnetic energy during any one event. A field which is stronger in the core of the star than the poloidal component we see on the surface is one solution to this problem. Another possible solution is that the field is very non-axisymmetric, and that the dipole measured is an underestimate of the average field strength on the surface. Any of these are also potential solutions to the phenomenon of NSs with very different observational properties which occupy the same region on the P–$\dot{P}$ diagram and have therefore the same dipole field strength.

Another effect that the magnetic field has is to deform the star's mass distribution. In the light of results presented above, it seems likely that a star has a predominantly toroidal field, deforming the star into a prolate shape. This causes the star to undergo torque-free precession and the damping of this precession will cause the star's magnetic axis to tend towards orthogonality with the rotation axis. In NSs, this could potentially happen fairly quickly, faster than the orientation of the axes can be changed by spin-down torque, which acts on the spin-down time-scale. In the millisecond magnetar models, the protoneutron star rotates at some significant fraction of break up and this results in a powerful dynamo which creates a strong magnetic field during the first hundred seconds. Since it seems very likely that the equilibrium formed after this dynamo switches off is predominantly toroidal, the star should flip over and emit gravitational waves observable with the next generation of detectors at least as far away as the Virgo cluster. However, the spin-down time-scale of a NS rotating with $P = 1$ ms and $B = 10^{15}$ G is only an hour, so the flipping over mechanism has to work fairly fast. Since the free precession period of such a star would be $P/\epsilon = 1000$ s, where $\epsilon \sim 10^{-6}$ is the ellipticity induced by the magnetic field of this magnitude, the damping of the precession would have to be very efficient indeed unless the magnetic equilibrium could be produced already at an angle to the rotation axis. More work is required to address these issues.

ACKNOWLEDGMENTS

The author would like to thank Åke Nordlund and Henk Spruit for assistance and useful discussions, and Chris Thompson and Anna Watts for pointing out the importance of this problem.

REFERENCES

Akgün T., Link B., Wasserman I., 2006, MNRAS, 365, 653
Bernstein I. B., Frieman E. A., Kruskal M. D., Kulsrud R. M., 1958, Proc. Royal Soc. London Math. Phys. Sci., 244, 1236, 17
Bonanno A., Urpin V., 2008, A&A, 477, 35
Braithwaite J., 2006, A&A, 453, 687
Braithwaite J., 2007, A&A, 469, 275
Braithwaite J., 2008, MNRAS, 386, 1947 (Paper II)
Braithwaite J., Nordlund Å., 2006, A&A, 450, 1077 (Paper I)
Braithwaite J., Spruit H. C., 2004, Nat, 431, 891
Braithwaite J., Spruit H. C., 2006, A&A, 450, 1097
Chandrasekhar S., Fermi E., 1953, ApJ, 118, 116
Cutler C., Ushomirsky G., Link B., 2003, ApJ, 588, 975
Duncan R. C., Thompson C., 1992, ApJ, 392, 9
Ferrario L., Wickramasinghe D. T., 2005, MNRAS, 356, 615
Ferrario L., Wickramasinghe D. T., 2006, MNRAS, 367, 1323
Frieman E. A., Rotenberg M., 1960, Rev. Mod. Phys., 32, 898
Gudiksen B. V., Nordlund Å., 2005, ApJ, 618, 1020
MacGregor K. B., Cassinelli J. P., 2003, ApJ, 586, 480
Markey P., Tayler R. J., 1973, MNRAS, 163, 77
Markey P., Tayler R. J., 1974, MNRAS, 168, 505
Mathys G., 2001, in Mathys G., Solanki S. K., Wickramasinghe D. T., eds, ASP Conf. Ser., Vol. 248, Magnetic Fields Across the Hertzsprung–Russell Diagram. Astron. Soc. Pac., San Francisco, p. 267
Mathys G., 2008, Contrib. Astron. Obs. Skalnaté Pleso, 38, 217
Mestel L., 1961, MNRAS, 122, 473
Mestel L., Nittmann J., Wood W. P., Wright G. A. E., 1981, MNRAS, 195, 979
Nordlund Å., Galsgaard K., 1995, preprint (http://www.astro.ku.dk/~aake/papers/95.ps.gz)
Pitts E., Tayler R. J., 1986, MNRAS, 216, 139
Prendergast K. H., 1956, ApJ, 123, 498
Roxburgh I. W., 1966, MNRAS, 132, 347
Spruit H. C., 1998, A&A, 333, 603
Spruit H. C., 1999, A&A, 349, 189
Tayler R. J., 1957, Proc. Phys. Soc. B, 70, 311957
Tayler R. J., 1973, MNRAS, 161, 365
Wasserman I., 2003, MNRAS, 341, 1020
Wentzel D. G., 1961, ApJ, 133, 170
Wickramasinghe D. T., Ferrario L., 2005, in Koester D., Moehler S., eds, ASP Conf. Ser. Vol. 334, White Dwarfs. Astron. Soc. Pac., San Francisco, p. 153
Woods P. M., Thompson C., 2004, preprint (astro-ph/0406133)
Wright G. A. E., 1973, MNRAS, 162, 339

This paper has been typeset from a TEX/LATEX file prepared by the author.